Current Progress in Rheology of Cellulose Nanofibril Suspensions

Oleksandr Nechyporchuk, Mohamed Naceur Belgacem, Frédéric Pignon

Review

Current progress in rheology of cellulose nanofibril suspensions

Oleksandr Nechyporchuk, Mohamed Naceur Belgacem, and Frédéric Pignon

Biomacromolecules, **Just Accepted Manuscript** • DOI: 10.1021/acs.biomac.6b00668 • Publication Date (Web): 16 Jun 2016

Current progress in rheology of cellulose nanofibril suspensions

Oleksandr Nechyporchuk,[†,*] *Mohamed Naceur Belgacem,*[‡] *Frédéric Pignon*[§]

[†] Chalmers University of Technology, Department of Chemistry and Chemical Engineering, Division of Applied Chemistry, SE-412 96 Gothenburg, Sweden.

[‡] Université Grenoble Alpes, Centre national de la recherche scientifique (CNRS), Laboratory of Pulp and Paper Science and Graphic Arts (LGP2), Agefpi, F-38000 Grenoble, France.

[§] Université Grenoble Alpes, Centre national de la recherche scientifique (CNRS), Laboratoire Rhéologie et Procédés (LRP), F-38000 Grenoble, France.

KEYWORDS: Rheological properties, cellulose nanofibrils, nanofibrillated cellulose, microfibrillated cellulose, fibrous suspensions, shear flow

ABSTRACT: Cellulose nanofibrils (CNFs) are produced and commonly used in the form of aqueous suspensions or gels. A number of studies have focused lately on rheological properties of CNF suspensions, which gives an insight into properties of such materials as well as can reflect their behavior during handling. This review summarizes the recent progress in rheological studies on CNF aqueous suspensions using rotational rheometry. Here, we discuss linear viscoelastic properties, *i.e.*, frequency-dependent storage and loss moduli; shear flow behavior,

i.e., apparent viscosity and shear stress as a function of shear rate; local flow characteristics etc. In this review, we point out that the rheological behavior of at least two types of CNF suspensions should be distinguished: (i) ones produced using mechanical fibrillation with or without enzymatic pretreatment (no surface chemical modification), which possess highly flocculated structure and (ii) ones produced involving chemical modification pretreatments, *e.g.*, carboxylation, carboxymethylation, quaternization or sulfonation, which possess better colloidal stability and do not evidently flocculate.

1. Introduction

The ongoing development of nanotechnology has led to the emergence of cellulose nanomaterials, which are produced from renewable resources and can serve the design of novel sustainable solutions for materials of the future. Nanocellulose has gained significant interest lately due to its renewable and biodegradable character, mechanical and colloidal properties, low density, useful optical properties *etc*. Nanocellulose is a family of materials that represents individualized cellulose particles with at least one dimension in nanoscale (1–100 nm). Two main families of nanocellulose include (i) cellulose nanocrystals (CNCs), also known as nanocrystalline cellulose or cellulose whiskers and (ii) cellulose nanofibrils (CNFs), also referred to as nanofibrillated cellulose (NFC), microfibrillated cellulose (MFC) or cellulose filaments.[1–3]

CNFs are flexible elongated particles (see Table 1) commonly extracted from wood and plants using mechanical disintegration in aqueous medium, which reduces interfibrillar interactions and yields highly viscous colloidal aqueous suspensions at low solids content, *e.g.*, at 1–2 wt.%.[4,5] Such viscous suspensions are formed due to the hygroscopic character of cellulose as well as the

high aspect ratio and the high specific surface area of the nanofibrils, resulting in their strong interconnections at low concentrations. The production of CNFs using only mechanical treatment is highly energy consuming. Thus, the development of pretreatment techniques, *e.g.*, enzymatic hydrolysis[6–8], carboxymethylation[9], carboxylation[10–12], quaternization[13,14] (with quaternary ammonium compounds) and sulfonation[15,16], has increased the interest in CNFs greatly, as summarized recently by Nechyporchuk *et al.*[4]

Table 1 Some properties of cellulose nanofibrils (CNFs)

Property	Value	Reference
Shape	Flexible elongated nanofibrils	6–23
Thickness, nm		
− no /enzymatic pretreatment	10–100	7,17–19
− chemical pretreatment	3−10	10,11,20
Length, nm		
− no /enzymatic pretreatment	1000–5000	18,21
− chemical pretreatment	500−2000	11,22
Crystallinity, %	40–80	12,18–20
Degree of polymerization	200–1000	11,18,19,23
Production yield, %	90–100	10,12

The applied production process influences strongly the final properties of CNF suspensions, including rheological behavior that can reflect the behavior of such suspensions during various processes, such as pumping, mixing or coating. CNFs produced using mechanical disintegration with or without enzymatic pretreatment (see Figure 1a) commonly have higher thickness and length compared to those obtained using chemical pretreatments (see Figure 1b).[19,24] Without chemical pretreatment CNFs usually possess agglomerated (flocculated) nature (see Figure 1c).

Some water release from such suspensions with high solids content (≥2 wt.%) occurs on storing. Chemical pretreatments are performed in order to introduce strong anionic (in case of carboxymethylation, carboxylation and sulfonation) or cationic (quaternization) charge on the surface, which causes electrostatic repulsion between the nanofibrils with same charges and hinders hydrogen bonding and van der Waals interactions. Mechanically disintegrated CNFs have only a slight negative charge originated from the presence of hemicellulose (*e.g.*, uronic acids). Chemically modified CNFs are usually not agglomerated (see Figure 1d), well dispersed and more colloidaly stable.[19] Some microstructural physical entanglements may still be present in these suspensions. Meanwhile, among all the types of produced CNFs there can be some portion of non-fibrillated residual fiber fragments.

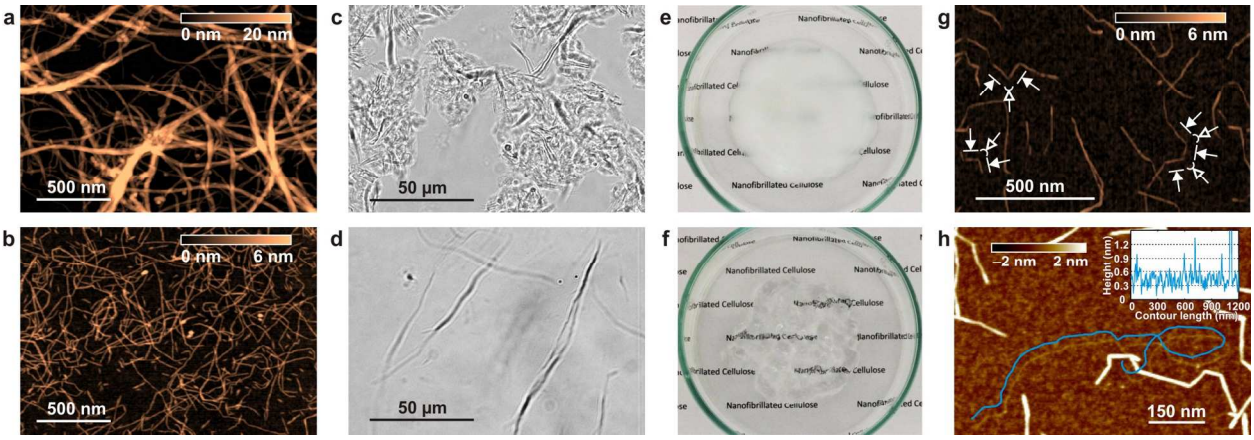

Figure 1 Properties of cellulose nanofibrils (CNFs) and their suspensions. AFM height images of CNFs produced using mechanical disintegration (**a**) without chemical pretreatment and (**b**) with carboxymethylation pretreatment, showing much smaller lateral dimensions of the latter (both adapted from ref. [24], the images were kindly provided by Tiina Pöhler (VTT, Finland)); optical microscope images of CNF suspensions produced (**c**) without chemical pretreatment and (**d**) with carboxylation *via* TEMPO-mediated oxidation pretreatment, showing the presence of agglomerated (flocculated) structures of the former and no agglomeration but only some rare

residual non-fibrillated fiber fragments of the latter (both adapted from ref. [19]. Copyright 2014 Springer Science+Business Media New York. With permission of Springer); Petri dishes with CNF suspensions produced using mechanical disintegration (**e**) without chemical pretreatment and (**f**) with carboxylation *via* TEMPO-mediated oxidation pretreatment, illustrating the much higher suspension transparency of the latter (both adapted from ref. [4]. Copyright 2016, with permission from Elsevier); (**g**) AFM height image with pointed (filled arrows) crystalline and (empty arrows) amorphous regions, resulting in flexible CNFs (adapted from ref. [24], the image was kindly provided by Tiina Pöhler (VTT, Finland)); (**h**) AFM height image of fully flexible single cellulose polymer chain with tracked contour shifted up for better visualization, an inset presents height profile along the tracked contour (adapted with permission from ref. [25]. Copyright 2015 Macmillan Publishers Limited).

Mechanical fibrillation yields nanofibrils that represent bundles of elementary fibrils and microfibrils, whereas CNFs produced with chemical pretreatments usually have smaller and a more uniform thickness, attributed to individual elementary fibrils. When elementary fibrils are extracted, cellulose crystalline (Figure 1g, filled arrows) and amorphous (Figure 1g, empty arrows) regions can be observed. In such elementary fibrils, cellulose polymer chains pass through several crystalline and amorphous regions. Therefore, the degree of polymerization of CNFs is commonly higher compared to that of cellulose nanocrystals, where the length of polymer chains is limited by the length of a single crystal, which is referred to as level-off degree of polymerization (LODP).

Elementary fibrils are considered as the smallest morphological units in the fiber cell wall.[26] It was reported previously that during nanocellulose production some peeling of molecularly thin sheets of cellulose can occur.[27–29] Recently, Usov et al.[25] showed that during CNF production with TEMPO-mediated oxidation pretreatment some single cellulose molecular chains (see Figure 1h) and 2 × 2 chain-packing structures are occasionally isolated. The corresponding height profile for single molecular chain is shown in the inset of Figure 1h. This work also confirmed the right-handed chirality of CNFs observed for both elementary fibrils and their bundles.

CNF suspensions form gels at low solids content when a critical concentration of the nanofibrils is surpassed.[6,30,31] Figure 1e,f show a visual aspect of CNF suspensions produced using enzymatic or 2,2,6,6-tetramethylpiperidine-1-oxyl (TEMPO)-mediated oxidation pretreatments, respectively, illustrating the much higher transparency of the latter due to lower lateral dimensions of the nanofibrils and, hence, lower light scattering. Additionally, high carboxylate content introduces electrostatic stabilization of CNFs by hindering their aggregation, which also reduces scattering of the suspensions.[20]Lately, a number of studies have been dealing with the rheological properties of CNF aqueous suspensions. Generally, they exhibit complex behavior and possess some typical features of soft glassy materials, such as clay suspensions, concentrated emulsions and colloidal gels, as well as typical behavior of colloidal and non-colloidal fiber suspensions, where the applied strain can disrupt and rearrange the materials structure.[32,33] CNF flocculation, orientation and migration from solid boundaries, as well as high time dependency of such systems complicates the rheological measurements.[34]

Some of these issues have been already addressed in review articles devoted to CNF production and their properties.[2,3,35] Several book chapters discussed certain issues related to the rheology of

CNF suspensions[36] or CNF-based composites.[37] Despite these good contributions, there is still a lack of extensive reviews addressing the challenges and summarizing the main outcomes in this field. Therefore, here we focus on the current progress in the rheology of CNF suspensions determined using rotational rheometry, particularly discussing the influence of the production processes, geometry shape and geometry gap and the issues of flow instabilities (wall-slip and shear banding).

2. Linear viscoelastic properties

CNF suspensions form network structures at low solids contents. Oscillatory shear measurements are usually performed for studying the linear viscoelastic properties of these structures. Oscillatory strain sweeps are executed to determine the linear viscoelastic regions, i.e., strain domains where storage (G') and loss (G'') moduli (dynamic moduli) are independent of strain. The oscillatory frequency measurements are then performed at a strain, which lies in the linear viscoelastic region.

An example of linear viscoelastic measurements for TEMPO-oxidized CNF suspensions at various concentrations (0.5–1.5 wt.%) is shown in Figure 2.[38] The linear behavior of the dynamic moduli in Figure 2a indicates strain domains where the elastic structure of CNF suspensions remains stable, which corresponds to linear viscoelastic regions. After exceeding a critical strain (*ca.* 1%), the elastic CNF network is destroyed, which is reflected by a non-linear behavior of the dynamic moduli.

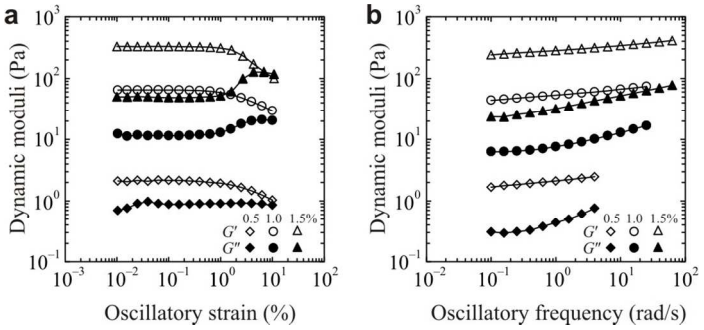

Figure 2 Storage and loss moduli as a function of: (**a**) oscillatory strain and (**b**) oscillatory frequency for TEMPO-oxidized NFC suspensions at different concentrations (0.5–1.5 wt.%), measured using Couette geometry (adapted from ref.[38]. Copyright 2015 Springer Science+Business Media Dordrecht. With permission of Springer).

Even at low concentrations CNF suspensions form gels, as shown in Figure 2b, which is reflected by $G' > G''$, G′ and G″ practically parallel to each other and largely frequency independent, *i.e.*, G' and $G'' \propto \omega^0$. Such gel-like properties were reported for CNF suspensions at as low concentration as 0.125 wt.%,[6] which corresponds to the gelation point, after which the nanofibrils start to form an interconnected network. As the concentration of CNFs increases, a stronger fibrous network is formed, which results in an increase of the dynamic moduli, which was extensively reported in different studies.[39–44]

NFC suspensions exhibit power law behavior, $G' \propto c^n$, where c is cellulose concentration, in the linear viscoelastic region when a percolated network is formed. The broad range of n values was reported in the literature: 2.25,[45] 2.4,[46] 2.5,[47] *ca.* 3,[6] 4.1,[48] 4.5,[49] and 5.2[31] for different types of CNF suspensions. Some of these values are considerably larger than those proposed by models for the elastic modulus of fibrous gels and semiflexible biopolymers as a function of

concentration, which yield power law exponents of 2−2.5.[50,51] More recently, Hill[52] proposed a new scaling theory for the elastic modulus of CNF suspensions that exhibits the transition from a power-law exponent of 11/3 to 7 when increasing cellulose volume fraction.

The network strength depends strongly on the type of pretreatment and on the extent of mechanical fibrillation used to produce CNFs. Chemically pretreated CNF suspensions usually have stronger network properties compared to enzymatically hydrolyzed or just mechanically fibrillated ones at equivalent concentrations.[36,43] This is explained by a higher specific surface area of the former and, hence, a higher degree of entanglement, despite the presence of a strong electrostatic repulsion between the nanofibrils. Therefore, TEMPO-oxidized CNF suspensions are commonly handled at 1 wt.%, whereas enzymatically hydrolyzed ones are processed at 2 wt.%, resulting in rather similar gel strength. Additionally, comparing to CNCs, which are rigid rod-like particles, CNFs form stronger networks at similar concentrations due to higher aspect ratio and ability to form physically entangled structures of flexible nanofibrils.[6,53]

Linear viscoelastic measurements (as well as shear flow measurements, as will be discussed below) were reported to illustrate the level of fibrillation while passing from raw microscopic fibers towards nanofibrils. Saarinen et al.[54] showed that the storage modulus of mechanically disintegrated cellulose suspensions decreases when increasing the level of fibrillation in a microfluidizer. Shogren et al.[55] observed first an increase of the storage modulus at initial stages of fibrillation (1–2 passes), which was further progressively decreased (2–8 passes) when exposing the suspensions to a homogenizer. Similar behavior was reported by Benhamou et al.[56] when using TEMPO-mediated oxidation pretreatment. They demonstrated an increase of the storage modulus followed by a continuous decrease when increasing the level of oxidation and maintaining equivalent mechanical fibrillation. In all these works[54–56], plate-plate geometry was

used and no information was provided regarding the preshear operation before the measurements. Contrary to the above works, Taheri and Samyn[57] reported an increase of the storage modulus and its stabilization at a certain level when imposed to more intense mechanical fibrillation of non-pretreated cellulose, which was measured using concentric cylinder (Couette) geometry. Furthermore, Naderi and Lindström[36] demonstrated that the network strength of an enzymatically pretreated suspension increases when exposing to more severe fibrillation conditions when the preshear protocol was applied before the measurements, followed by rest. On the other hand, when no preshear was used, the opposite behavior was reported with a decrease of storage modulus as a function of applied mechanical fibrillation (see Figure 3). In this work, a Couette geometry was used for the measurements. The last mentioned works[36,57] are in line with the generally known gel formation when passing from pulp suspensions towards highly-viscous CNF suspensions.

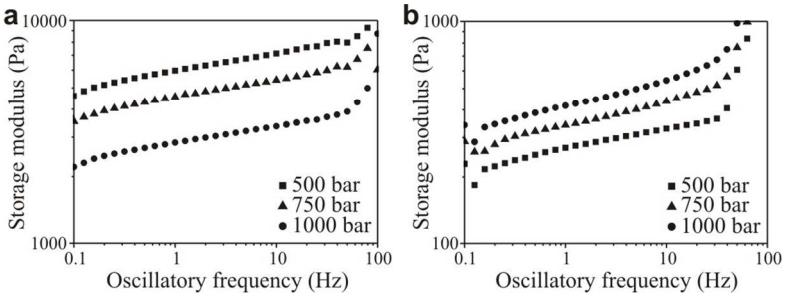

Figure 3 Storage modulus of enzymatically hydrolyzed CNF suspensions at 2 wt.% produced using homogenization at different applied pressures (**a**) without preshear and (**b**) with preshear protocol (adapted from ref. [36]. Copyright 2015, with permission from Nova Science Publishers, Inc.).

It should be mentioned that when using cone-plate and plate-plate geometries at initial stages of fibrillation, the measured response may originate from individual fibers and their entanglements, not from network structure of the suspension. This may result in much higher levels of measured dynamic moduli. On the other hand, such partially fibrillated suspensions are highly susceptible to sedimentation and depletion of the particles from the upper geometry wall in cone-plate and plate-plate geometries, typically yielding much lower values of the measured dynamic moduli due to lower elasticity in the depleted region. Concentric cylinder geometry with relatively wide gap appears to be much more reasonable for such measurements.

To study the possible influence of the rheometer geometry, Saarinen et al.[54] examined the influence of the geometry types (cone-plate, plate-plate and Couette) and geometry gap (in plate-plate) on the viscoelastic properties of mechanically fibrillated CNF suspensions. The highest level of storage modulus was reported for cone-plate, whereas the smallest one was observed for Couette geometry. It was also shown that the storage modulus decreases when increasing the distance between parallel plates (see Figure 4a). This difference becomes smaller when more fibrillated cellulose suspension is tested (see Figure 4b). These results are in line with the above discussion on the influence of large fibers and flocculated structures on the rheological measurements.

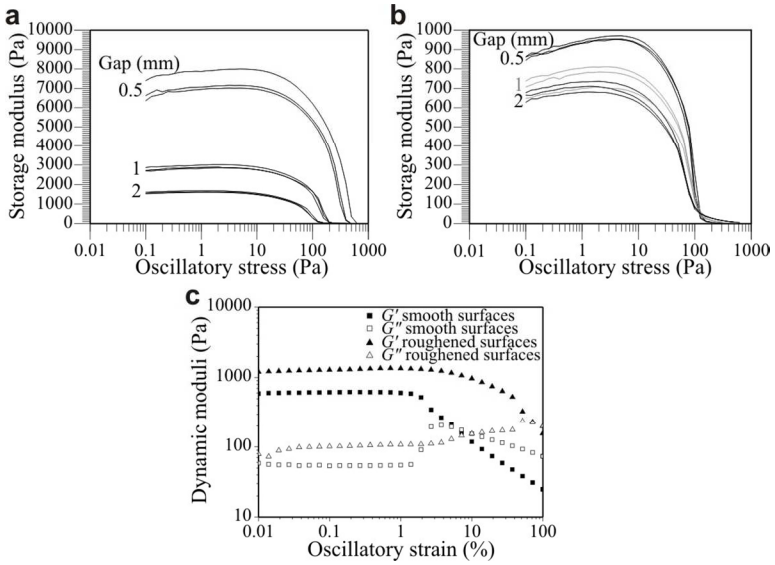

Figure 4 Effect of parallel plate geometry gap (0.5–2 mm) on storage modulus measurements (in triplicate) performed for mechanically fibrillated CNF suspensions at 2 wt.% produced applying: (**a**) lower and (**b**) higher level of fibrillation in a microfluidizer (both adapted from ref. [54], with permission from Annual Transactions of the Nordic Rheology Society); (**c**) dynamic moduli of 2 wt.% carboxymethylated CNF suspension measured using Couette with smooth and roughened surfaces (adapted from ref. [36]. Copyright 2015, with permission from Nova Science Publishers, Inc.).

Naderi and Lindström[36] demonstrated that it is necessary to use roughened (serrated / profiled) geometry surfaces when performing oscillatory measurements in order to hinder a slippage on the contact between geometry walls and the suspension (known as wall-slip or wall depletion). The wall-slip phenomenon is explained by the existence of thin lubricating layers on the boundary of the geometry surfaces in which the suspension structure is different from that in the bulk. Consequently, it was shown that the use of roughened geometries resulted in higher values

of the measured dynamic moduli, compared to those determined using smooth ones, as shown in Figure 4c.

It was also reported that there is almost no influence of temperature on the dynamic moduli of CNF suspensions that have been mechanically fibrillated[39] or enzymatically pretreated and fibrillated in a microfluidizer[6] (tested in the range of 25–60 °C or 20–80 °C, respectively). As the temperature increases, only a slight strengthening of the CNF network was observed. However, the gel strength can be controlled by adding salts in order to change the ionic strength. By increasing the ionic strength, stronger CNF networks are obtained due to screening of electrostatic interactions.[39,41,58,59] At the same time, however, this leads to higher CNF aggregation and lower colloidal stability. The presence of charged polymers, e.g., hemicellulose, contributes also to the electrostatic interactions of CNFs and influences the rheological behavior.[59]

In summary, it can be noted that when analyzing highly fibrillated CNF suspensions with negligible amount of residual fiber fragments, there may be an optimal production conditions, which result in the highest network properties. When subjecting these suspensions to further mechanical treatment, reduction of the CNF aspect ratio may occur[56], which can yield a lower network strength of the suspension. When chemical modification is applied to facilitate the nanofibril separation, reduction of the interfibrillar interactions can occur due to enhancement of the electrostatic repulsion and decrease of the magnitude of friction coefficient between the nanofibrils.[60] This may compete with the increase of cellulose specific surface area and with variations in aspect ratio. Thus, the CNF network strength can fluctuate depending on various parameters. As mentioned above, the preshear protocol, performed in order to eliminate the thixotropy effect, seems to alter the structure of CNF suspensions, resulting in different

measured properties compared to those obtained without the preshear step. The preshear may have much stronger effect on mechanically fibrillated CNF suspension produced with or without enzymatic pretreatment, which are highly flocculated.

3. Shear flow properties

Regardless of the production conditions, all types of CNF suspensions possess shear thinning properties, *i.e.*, their viscosity decreases with an increase of shear rate. They also are thixotropic, *i.e.*, their viscosity decreases when a steady shear rate is applied, reaching an equilibrium level, and viscosity rises back to the same level as for the suspension at rest, when the shear rate is reduced to zero. Therefore, due to huge time dependencies, the measurements should be performed at steady-state flow.

Shear flow measurements can serve as a tool for characterization of the degree of fibrillation similarly to the linear viscoelastic measurements, as discussed above. In the pioneering work of Herrick et al.[61], it was shown that viscosity of mechanically fibrillated CNF suspensions enhance progressively when increasing the number of passes in a homogenizer, measured using Couette geometry. They indicated that at highest levels of fibrillations, the flow curves were the least fluctuated due to less interference caused by pulp macrostructures. Grüneberger et al.[62] demonstrated the same tendency of viscosity increase when increasing number of passes through a grinder (see Figure 5a) or a microfluidizer, determined using Couette geometry. They also indicated, that the flow curves were very irregular at the initial stages of fibrillation using grinder, since phase separation in suspensions occurred. Therefore, this data was omitted for the analysis, and the viscosity at higher fibrillation levels was evaluated. Similar observations were reported by Taheri and Samyn[57] for mechanically fibrillated suspensions.

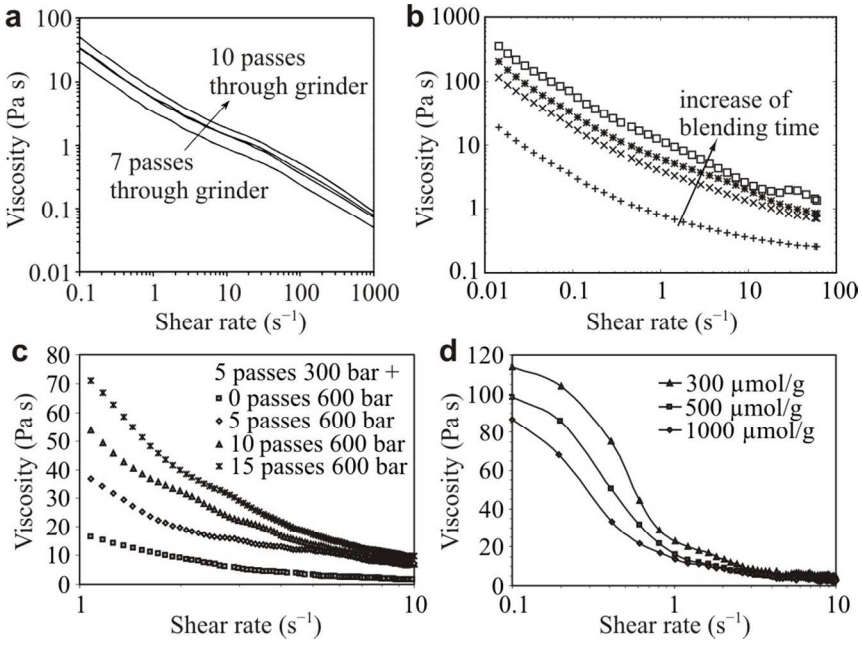

Figure 5 Effect of production conditions on the measured apparent viscosity of: (**a**) 1.8 wt.% CNF suspensions grinded different number of passes (adapted from ref. [62]. Copyright 2014 Springer Science+Business Media Dordrecht. With permission of Springer); (**b**) 0.4 wt.% TEMPO-oxidized CNF suspensions blended for various time (adapted from ref. [40]. Copyright 2007 Springer Science+Business Media B.V. With permission of Springer); (**c**) 1.5 wt.% TEMPO-oxidized CNF suspensions at various carboxyl content (TEMPO-oxidation), produced using homogenizer by 5 passes at 300 bar, and (**d**) TEMPO-oxidatized CNF suspension with carboxyl content of 1000 µmol/g, at various passes in a homogenizer (both adapted from ref. [63]. Copyright 2010, with permission from Elsevier).

An increase of the viscosity with an increase of fibrillation level was also reported for chemically pretreated CNF suspensions using TEMPO-mediated oxidation[40] (see Figure 5b) and carboxymethylation.[64] However, Besbes et al.[63] demonstrated that there is a difference in

viscosity tendency depending on variation of either mechanical fibrillation or oxidation levels, when using cone-plate geometry. Increase of number of passes in a homogenizer resulted in the increase of the viscosity (see Figure 5c), which is in agreement with the previous works. However, increase of carboxylate charge led to lower suspensions viscosity (see Figure 5d), which is in line with the decrease of dynamic moduli with an increase of oxidation level shown by Benhamou et al.[56], as discussed above.

Pääkkö et al.[6] demonstrated the influence of pH on the viscosity of enzymatically pretreated and disintegrated in a microfluidizer CNF suspension. They showed that reduction of the pH progressively from 10 to 2 resulted in the increase of the viscosity due to neutralization of some negative charge (due to the presence of hemicellulose) by hydrogen ions and enhancement of interfibrillar interactions.

It was also reported that the viscosity of CNF suspensions decreases with an increase of temperature (examined range of 20–80 °C[61] and 25–60 °C[65]), Interestingly, we have discussed above the opposite tendency for storage modulus.[6,39] This suggests the different behavior of the suspensions in linear viscoelastic region, where the CNFs are strongly interconnected, and at flow, where the nanofibril network is broken. Decrease of the viscosity with temperature increase is also known for aqueous solutions of carboxymethyl cellulose.[66]

Shear flow measurements of CNF suspensions in a dilute regime, where nanofibrils do not interact with each other, have attracted much attention lately as a tool to evaluate their aspect ratio.[67–71] These works were mostly focused on TEMPO-oxidized CNFs. The recent work of Tanaka et al.[71] showed that intrinsic viscosity of diluted CNF suspensions can be solely expressed as a function of aspect ratio of the nanofibrils, regardless of their flexibility.

Similarly to the dynamic moduli, both viscosity and shear stress increase as a function of CNF concentration.[40,41,63,65,72,73] As mentioned above, these suspensions possess shear thinning behavior, which is observed at wide range of shear rates. In a number of studies, a Newtonian plateau was reported between the low and high shear rate regions[46,64,74–77], and a hysteresis loop was observed when increasing-decreasing (or vice versa) the shear rate[36,65,76]. It is noteworthy that the Newtonian plateau and hysteresis were observed for CNF suspensions produced both without and with chemical pretreatments. However, these phenomena were much less pronounced for the latter. They were associated with formation and breakdown of shear-induced structures in CNF suspensions.

In order to study these structural changes in CNF suspensions under shear, Saarikoski et al.[58] and Karppinen et al.[75] used a visualization setup consisting of Couette geometry with transparent cup and a camera. Such a method yielded information about the CNF structure at the outer geometry wall. In their work, flocculation of CNF suspensions produced using mechanical disintegration was examined. They studied the suspensions after preshear and recovery intervals to introduce comparable shear history.

It was shown that mechanically fibrillated CNF suspensions are present in the form of sintered flocs. At low apparent shear rates, their structure breaks into rolls that are elongated along the Couette height, forming chain-like structures. At the intermediate shear rates, the floc rolls start to separate into individual spherical flocs. Finally, at high shear rates, CNFs flow in the detached flocs, size of which changes inversely proportional to the shear rate (see Figure 6a–c). It was also shown that this transition in floc structures is reversible when the shear rate is decreased back [58]. However, the measured shear stress was slightly lower typically at low shear rates at the back

ramp. Thus, it was assumed that high shear rates in the rheometer might cause some irreversible aggregation of the CNF network.

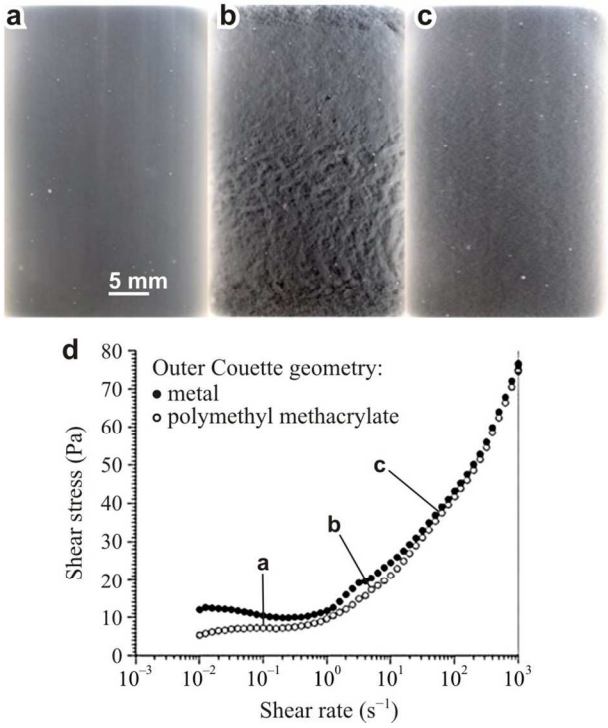

Figure 6 Photographs showing a structure of mechanically fibrillated CNF suspensions at 1 wt.% at the outer Couette surface at the shear rates of 0.1 s^{-1} (**a**), 5.0 s^{-1} (**b**) and 63.1 s^{-1} (**c**); the inner cylinder rotates to the left; and the corresponding flow curves (**d**) measured using geometries with different outer geometry surfaces (adapted from ref. [75]. Copyright 2012 Springer Science+Business Media B.V. With permission of Springer).

Additionally, Saarikoski et al.[58] have pointed out the dependence of floc size on the geometry gap (0.9 and 1.3 mm, by changing Couette geometries). The larger floc dimensions were observed when using lower geometry gap. It was assumed that lower geometry gap limits the

stress transfer in the bulk of suspension, hindering the breakdown of the flocs. Thus, it was assumed that the measurements at lower geometry gap were more influenced by wall-slip.

The wall-slip is known to take place in fibrous suspensions[78]. It occurs due to displacement of a dispersed phase from geometry boundaries, which creates a lubrication layer. In this layer, the suspension structure is different from that of in the bulk. Lasseuguette et al.[40] used birefringence measurements to demonstrate the alignment of TEMPO-oxidized nanofibrils under shear. Thus, shear-induced orientation of CNFs can serve as one of the possible explanations of the wall-slip occurrence.

Comparing to mechanically disintegrated CNFs, chemically oxidized ones do not exhibit evident flocculation. Thus, the structural changes at intermediate shear rates may not occur for the second type of CNF suspensions. However, Lasseuguette et al.[40] showed a drastic change in orientation angle of TEMPO-oxidized CNFs in the range of 30–40 s^{-1}, revealing the structural changes of the suspension network in this shear rate domain, suggesting that some microstructural changes of CNF structure occur. It was also shown that increase of the oxidation level reduces the flocculation of CNFs.[76]

Martoïa et al.[33] compared the flow behavior of CNF suspensions, produced employing either enzymatic pretreatment or TEMPO-mediated oxidation, using visualization approach. They observed flocculated behavior of the enzymatically hydrolyzed suspensions with viscosity plateaus associated to drastic structural changes in the suspension. Similarly to the above works[58,75], the CNF suspension was in the form of floc chains (100–300 μm), which split into individual flocs (<100 μm) as the shear rate increased. Whereas TEMPO-oxidized CNF suspension was non-flocculated both at rest and during shearing. However, the flow curves still

displayed some sudden slope changes, which were assumed to be associated with inhomogeneous flow, *i.e.*, wall-slip and flow localization within specific sample volume (shear banding).

Additionally, for both types of CNF suspensions, flow curves did not superimpose when subjected to upward and followed by downward shear rate sweeps. The differences of flow curves were larger at lower shear rates. However, the curves superimposed well both at very low and high shear rates when first decreasing and then increasing the shear rate for both types of the suspensions.

Naderi et al.[31] suggested the presence of some small-size aggregates when studying rheology of carboxymethylated NFC, which was evident at very low solids concentrations below the nanofibril percolation threshold. Thus, the above observations of Lasseuguette et al.[40] and Martoïa et al.[33] may be associated with separation of several interconnected (or breakdown of single) aggregates.

Summarizing above, it should be noted that when performing the rheological measurements at least two types of CNF suspensions should be distinguished: (i) ones prepared using mechanical disintegration with or without enzymatic pretreatment, which results in strong flocculated structures having a size of several hundreds of micrometers, where agglomeration is caused by hydrogen bonding and van der Waals interactions and (ii) ones produced with chemical pretreatments, which introduce repulsive electrostatic forces between the nanofibrils and results in more colloidaly stable and practically non-flocculated suspensions. Some flocculation can still occur at low degrees of substitution of the chemically modified cellulose. For the first type of CNF suspensions, any analysis of the flow properties should be considered cautiously, since the

size of the flocs is in the same order of magnitude as the geometry gap. Moreover, such suspensions are prone to phase separation. Since cone-plate and plate-plate geometries are more influenced by wall-slip at upper geometry surface, it can result in higher errors in the measured rheological properties. Therefore, concentric cylinder geometries with relatively wide gap can reduce the impact of these shortcomings.

4. Local flow properties

The conventional flow measurements revealed the complex flow behavior of CNF suspensions. Actually, suspensions, being two-phase fluids, typically undergo non-homogeneous (non-laminar) flow, which is characterized by coexistence of multiple flow bands[79], *i.e.*, the regions with different velocity; wall-slip,[78] *i.e.*, depletion of suspension particles near the geometry walls that creates less viscous regions *etc*. These flow instabilities can introduce errors and difficulties in the results interpretation. Thus, local flow measurements based on determination of the velocity profile within the geometry gap can provide evidence of multiple flow regimes in CNF suspensions and suggest more accurate results characterization.

A simple methodology to monitor a strain field in the geometry gap and to detect the possible flow instabilities was proposed by Nechyporchuk et al.[43] In that work, the cone was pierced close to the outer edge, which allowed introducing a thin colored vertical filament in the bulk of CNF suspension and to analyze the filament deformation when performing the flow measurements using cone-plate geometry (see Figure 7a). As a filament, the same CNFs as tested but colored with titanium dioxide pigment was used. Due to the filament introduction, it was not possible to perform the measurements just after the preshear; therefore, the measurements in a steady state

regime were carried out in order to eliminate the effect of thixotropy. Such an approach is quite easy and allows fast detection of the wall-slip and flow localization through visual observation.

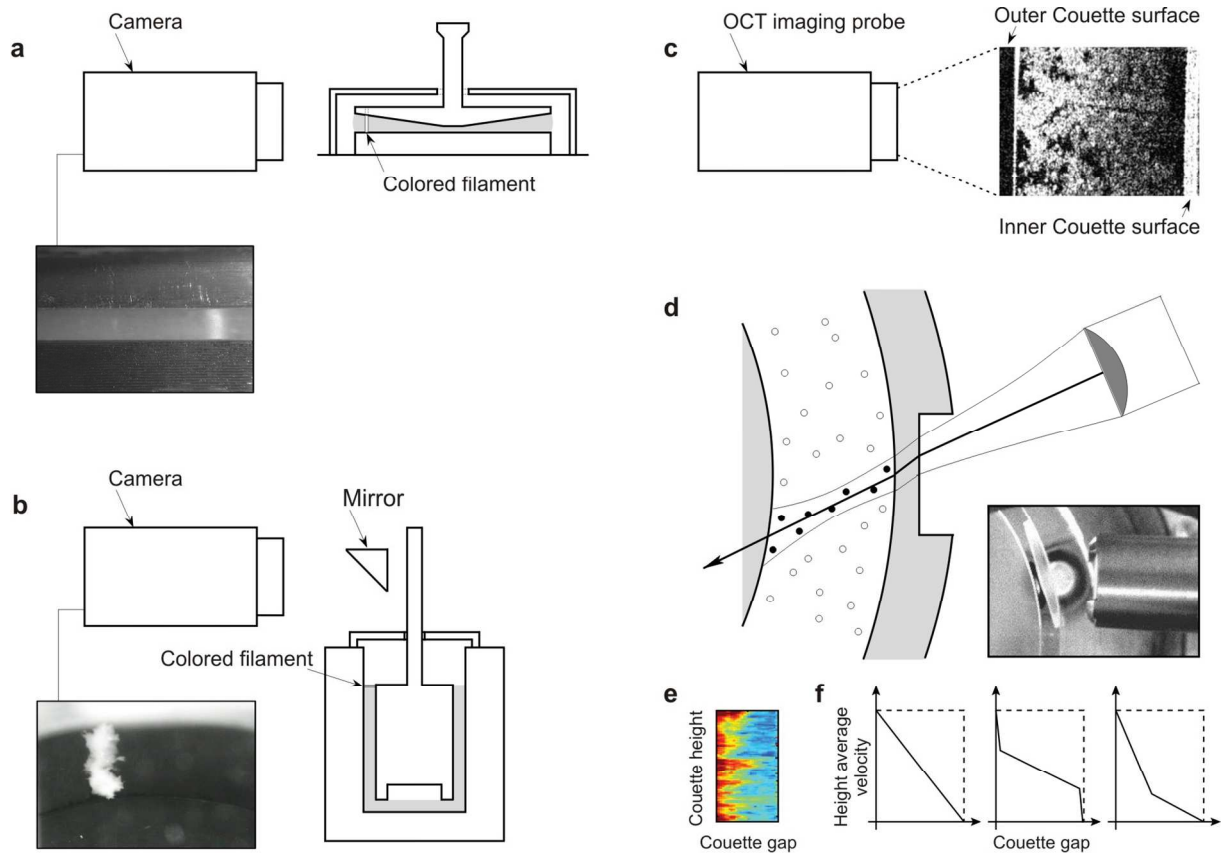

Figure 7 Local flow rheology measurement setups: based on the introduction of filament of CNFs colored by titanium dioxide in CNF bulk and measurements using (**a**) cone-plate (adapted from ref. [43]. Copyright 2014, with permission from Elsevier) and (**b**) Couette geometries (adapted from ref. [38]. Copyright 2015 Springer Science+Business Media Dordrecht. With permission of Springer); (**c**) optical coherence tomography (OCT) combined with Couette rheometry (adapted from ref.[77]. Copyright 2014 Springer Science+Business Media Dordrecht. With permission of Springer); (**d**) ultrasonic speckle velocimetry (USV) setup combined with Couette rheometry (adapted with permission from ref. [80]. Copyright 2004 EDP Sciences), which allows recording of (**e**) velocity maps (adapted from ref. [33]. Copyright 2015, with permission of

The Royal Society of Chemistry. http://dx.doi.org/10.1039/c5sm00530b) and measuring of (**f**) height average velocity profiles, showing examples of (*left*) laminar flow, (*middle*) slippage at the walls and (*right*) shear bending (adapted with permission from ref. [80]. Copyright 2004 EDP Sciences).

It was shown[43] that the use of smooth geometry surfaces resulted in a strong impact of wall-slip at low shear rates for both enzymatically hydrolyzed (at 2 wt.%) and TEMPO-oxidized (at 1 wt.%) CNF suspensions. The slippage occurred at the boundary between the CNF suspension and the cone or at the two boundaries between the suspension and both the cone and the plate. When roughened cone and plate were applied, no evident slippage was observed in the case of TEMPO-oxidized CNFs, which led to an increase of the shear stress at low shear rates, compared to that measured using the non-roughened surfaces. Whereas, in case of enzymatically hydrolyzed CNFs, the roughened geometry surfaces resulted in lower shear stress at moderate shear rates that was influenced by flocculation, sedimentation of flocs and water release from the suspension, which was induced by rough geometry surfaces.

This concept of strain field examination was later implemented by Nechyporchuk et al.[38] in concentric cylinders with smooth and serrated surfaces and vane-in-cup geometry. As an example, Figure 7b illustrates the Couette system developed in their work. It was reported that the flow curves depend strongly on the used geometry at low shear rates (see Figure 8), where the wall-slip plays a significant role. However, at high shear rates there is no influence of the applied geometry, resulting in similar values of shear stress. The slippage becomes more crucial

as the solids content of the suspension increases. Roughened Couette geometry was found to be efficient to compete with the wall-slip at low shear rates.

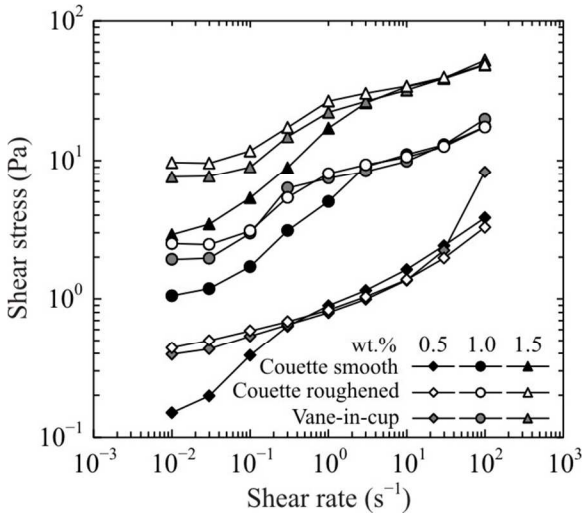

Figure 8 Comparison of the flow curves of TEMPO-oxidized NFC suspensions at various concentrations using different geometries (adapted from ref.[38]. Copyright 2015 Springer Science+Business Media Dordrecht. With permission of Springer).

More complex techniques for the analysis of local flow properties of CNF suspensions were reported based on combination of flow measurements with an optical coherence tomography (OCT),[77,81] ultrasonic speckle velocimetry (USV)[33] or magnetic resonance imaging (MRI),[82] which give possibility to measure real velocity profile across the rheometer gap. For instance, USV (see Figure 7d) can be used to determine a velocity map inside the Couette (see Figure 7e) and to measure height average velocity profile as a function of the geometry gap (see Figure 7f). The velocity profile can finally give an evidence of either homogeneous flow (Figure 7f, left), slippage on the walls (Figure 7f, middle), or shear bands coexisting in the gap (Figure 7f right).

The use of OCT to measure the local rheology of mechanically fibrillated CNF suspensions was reported by Saarinen et al.[77] and Haavisto et al.[81] OCT allowed real-time imaging of the internal structure of the suspension in the Couette gap and measurement of the radial mean velocity profile by tracking the displacement of CNF flocs (see Figure 7c). At high shear rates, the floc size was found to decrease as the shear rate increased. In this region, the apparent shear thinning was believed to represent the adaptation of the floc structure to the apparent shear rate. Whereas at low shear rates the flocs stuck to each other resulting in more significant wall-slip, which was increased even more by decreasing the CNF concentration or increasing the ionic strength by adding sodium chloride due to creation of rotating floc structures and decreasing the amount of water held by the CNF network. In this shear rates region, the apparent shear thinning did not reflect structural changes in the bulk, but represented the shear thinning in the slippage layer or shear thinning combined with an increase of the size of flocs and their movement. Haavisto et al.[81] showed that shear flow measurements only at high shear rates closely represent the bulk properties of CNF suspensions, which is in accordance with the above discussed studies[38,43].

In addition to the visual observation of the CNF structure discussed above, Martoïa et al.[33] compared the rheological behavior of enzymatically hydrolyzed and TEMPO-oxidized CNF suspensions using Couette geometry combined with USV. In their work, it was shown that for both types of CNF suspensions the flow was affected by the presence of wall-slip and multiple flow bands, which evolved with applied shear rate.

The examination of enzymatically pretreated CNF suspensions showed the presence of individual flocs and floc chains, which is in line with the previous studies.[58,75,77] Owing to such a complex structure, these suspensions exhibited a heterogeneous velocity over the entire height of

the Couette. The height average velocity profiles at different times of steady shear (Figure 9a) also demonstrate the heterogeneous (non-laminar) flow within the Couette gap. After several tens of seconds, the velocity profile tends to stabilize, showing the presence of (i) a slippage on the rotor, where the velocity is twice lower than for the theoretical profile, (ii) a velocity plateau close to the stator, indicating that the suspension is not sheared properly in this gap domain and (iii) a slippage on the stator, where the velocity is higher than for the theoretical profile.

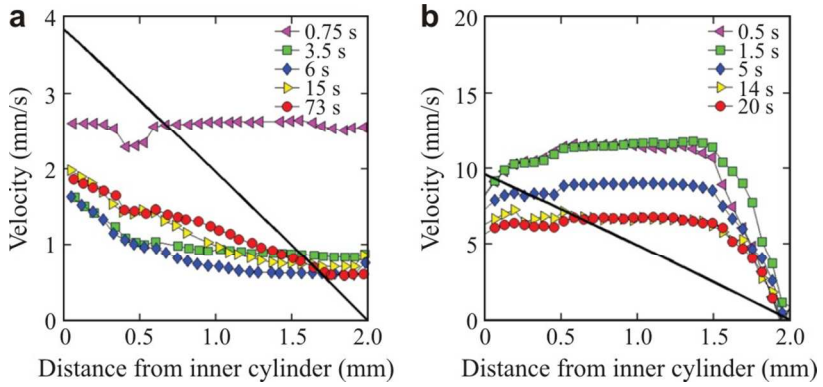

Figure 9 Height average velocity profiles at different times of applied shear for (**a**) enzymatically hydrolyzed CNF suspension at a concentration of 2 wt.%, applied shear rate of 2 s^{-1} and (**b**) TEMPO-oxidized CNF suspension at a concentration of 1 wt.%, applied shear rate of 5 s^{-1}. On the abscissa axis, 0 and 2 mm correspond to inner and outer Couette surfaces, respectively. Solid lines represent a theoretical profile at a given shear rate in case of laminar flow (adapted from ref. [33]. Copyright 2015, with permission of The Royal Society of Chemistry. http://dx.doi.org/10.1039/c5sm00530b).

For the TEMPO-oxidized CNF suspension, no noticeable heterogeneities were observed within the height of the Couette and no slippage on the stator was observed from the height average

velocity profiles (see Figure 9b). However, still there was a slippage on the rotor wall and a broad plateau of the constant velocity in the Couette gap, where the suspension was not properly sheared. No distinct variation in the suspension structure was observed; however, some microstructural changes in the CNF network might occur, related to the shear localization.

De Kort et al.[82] used rheo-MRI velocimetry, applying smooth cone-plate geometry, to measure flow profiles of CNF suspensions with adsorbed carboxymethyl cellulose produced by homogenization of bacterial cellulose. They demonstrated non-linear flow behavior with a presence of slippage on plate surface, associating the above phenomena with CNF flocculation and possible migration of flocs under shear.

In summary, the local flow measurements showed that during the rheological measurements the CNF suspensions are very weakly sheared at low shear rates. More accurate rheological data can be extracted from high shear rates (10–100 s^{-1}), where the influence of wall-slip and shear banding is minimized. At the same time, such flow instabilities is an inherent property of CNF suspensions, which demonstrates how they can behave for instance in contact with smooth or rough surfaces.

Conclusions and Future Perspectives

Rheology of CNF suspensions plays an important role for achieving efficient pumping, mixing or coating of this material during production process or its various applications. CNFs in aqueous medium form interconnected networks, which exhibit gel-like, shear thinning and thixotropic behavior. The strength of these networks is increased with higher cellulose concentration and with higher ionic strength. With an increase of temperature, the strength of CNF suspensions

remains practically unchanged in the linear viscoelastic region; however, during flow measurements their viscosity decreases.

At least two types of CNF suspensions should be distinguished depending on the production method: (i) fibrillated mechanically with or without enzymatic pretreatment and (ii) fibrillated mechanically with preliminary chemical surface modification that introduces strong electrostatic repulsion between nanofibrils.

The first type of CNF suspensions has a flocculated nature. The size of these flocs reach several hundreds of micrometers. Thus, interpretation of the measurements using cone-plate or plate-plate geometries should be cautious, since the size of the flocs is in the same order of magnitude as the geometry gap (this is also relevant for partially fibrillated pulp suspensions). These suspensions are more prone to phase separation and wall depletion. Wide-gap Couette geometries with roughened surfaces are thus considered as more convenient for the rheological measurements of this type of CNFs.

The second type of CNF suspensions is more colloidaly stable due to smaller nanofibril dimensions. These suspensions are more viscous at equivalent concentrations due to higher level of interconnection between the nanofibrils. Such suspensions are typically non-flocculated; however, they still have some imperceptible small-size aggregates. These CNF suspensions are less influenced by geometry gap, however, are still susceptible to wall depletion. Thus, geometries with roughened surfaces are more convenient to hinder these effects.

Flow instabilities are typical for both types of CNF suspensions and are more pronounced at high suspension solids content. At high shear rates (10–100 s^{-1}) the measurements are much less influenced by the flow instabilities as well as the used geometries and their roughness. Thus,

flow measurements using rotational rheometer correspond better to CNF suspension properties at high shear rates.

As research activities continue, it is still necessary to establish reliable methodologies for rheological characterization of different types of CNF suspensions, taking into account geometry types, surface roughness, gap *etc*. This will allow comparing various systems studied by different research groups. Further work should also be aimed at developing ways to rapidly tune the rheological behavior of CNF suspensions for the desired applications.

AUTHOR INFORMATION

Corresponding Author

* E-mail: o.nechyporchuk@gmail.com.

ACKNOWLEDGMENT

LRP and LGP2 are both a part of the LabEx Tec 21 (Investment for the Future, Grant Agreement No. ANR-11-LABX-0030) and PolyNat Carnot Institute (ANR-11-CARN-030-01). LGP2 is also a part of the Énergies du Futur Carnot Institute (ANR-11-CARN-007-01).

REFERENCES

(1) Siró, I.; Plackett, D. *Cellulose* **2010**, *17* (3), 459–494.
(2) Klemm, D.; Kramer, F.; Moritz, S.; Lindström, T.; Ankerfors, M.; Gray, D.; Dorris, A. *Angew. Chem. Int. Ed.* **2011**, *50* (24), 5438–5466.
(3) Moon, R. J.; Martini, A.; Nairn, J.; Simonsen, J.; Youngblood, J. *Chem. Soc. Rev.* **2011**, *40* (7), 3941–3994.
(4) Nechyporchuk, O.; Belgacem, M. N.; Bras, J. *Ind. Crops Prod.* **2016**.
(5) Lindström, T.; Aulin, C.; Naderi, A.; Ankerfors, M. In *Encyclopedia of Polymer Science and Technology*; John Wiley & Sons, Inc., 2014.
(6) Pääkkö, M.; Ankerfors, M.; Kosonen, H.; Nykänen, A.; Ahola, S.; Österberg, M.; Ruokolainen, J.; Laine, J.; Larsson, P. T.; Ikkala, O.; Lindström, T. *Biomacromolecules* **2007**, *8* (6), 1934–1941.

(7) Henriksson, M.; Henriksson, G.; Berglund, L. A.; Lindström, T. *Eur. Polym. J.* **2007**, *43* (8), 3434–3441.
(8) Janardhnan, S.; Sain, M. M. *BioResources* **2007**, *1* (2), 176–188.
(9) Wågberg, L.; Decher, G.; Norgren, M.; Lindström, T.; Ankerfors, M.; Axnäs, K. *Langmuir* **2008**, *24* (3), 784–795.
(10) Saito, T.; Nishiyama, Y.; Putaux, J.-L.; Vignon, M.; Isogai, A. *Biomacromolecules* **2006**, *7* (6), 1687–1691.
(11) Saito, T.; Hirota, M.; Tamura, N.; Kimura, S.; Fukuzumi, H.; Heux, L.; Isogai, A. *Biomacromolecules* **2009**, *10* (7), 1992–1996.
(12) Liimatainen, H.; Visanko, M.; Sirviö, J. A.; Hormi, O. E. O.; Niinimaki, J. *Biomacromolecules* **2012**, *13* (5), 1592–1597.
(13) Ho, T. T. T.; Zimmermann, T.; Hauert, R.; Caseri, W. *Cellulose* **2011**, *18* (6), 1391–1406.
(14) Liimatainen, H.; Suopajärvi, T.; Sirviö, J.; Hormi, O.; Niinimäki, J. *Carbohydr. Polym.* **2014**, *103*, 187–192.
(15) Liimatainen, H.; Visanko, M.; Sirviö, J.; Hormi, O.; Niinimäki, J. *Cellulose* **2013**, *20* (2), 741–749.
(16) Sirviö, J. A.; Kolehmainen, A.; Visanko, M.; Liimatainen, H.; Niinimäki, J.; Hormi, O. E. O. *ACS Appl. Mater. Interfaces* **2014**, *6* (16), 14384–14390.
(17) Turbak, A. F.; Snyder, F. W.; Sandberg, K. R. *J. Appl. Polym. Sci. Appl. Polym. Symp.* **1983**, *37*, 815–827.
(18) Iwamoto, S.; Nakagaito, A. N.; Yano, H.; Nogi, M. *Appl. Phys. A* **2005**, *81* (6), 1109–1112.
(19) Nechyporchuk, O.; Pignon, F.; Belgacem, M. N. *J. Mater. Sci.* **2015**, *50* (2), 531–541.
(20) Besbes, I.; Vilar, M. R.; Boufi, S. *Carbohydr. Polym.* **2011**, *86* (3), 1198–1206.
(21) Stelte, W.; Sanadi, A. R. *Ind. Eng. Chem. Res.* **2009**, *48* (24), 11211–11219.
(22) Liimatainen, H.; Ezekiel, N.; Sliz, R.; Ohenoja, K.; Sirviö, J. A.; Berglund, L.; Hormi, O.; Niinimäki, J. *ACS Appl. Mater. Interfaces* **2013**, *5* (24), 13412–13418.
(23) Shinoda, R.; Saito, T.; Okita, Y.; Isogai, A. *Biomacromolecules* **2012**, *13* (3), 842–849.
(24) Pöhler, T.; Lappalainen, T.; Tammelin, T.; Eronen, P.; Hiekkataipale, P.; Vehniäinen, A.; Koskinen, T. M. In *2010 TAPPI International Conference on Nanotechnology for the Forest Product Industry*; Finland, 2010.
(25) Usov, I.; Nyström, G.; Adamcik, J.; Handschin, S.; Schütz, C.; Fall, A.; Bergström, L.; Mezzenga, R. *Nat. Commun.* **2015**, *6*, 7564.
(26) Frey-Wyssling, V. A.; Mühlethaler, K. *Makromol. Chem.* **1963**, *62* (1), 25–30.
(27) Li, Q.; Renneckar, S. *Cellulose* **2009**, *16* (6), 1025–1032.
(28) Li, Q.; Renneckar, S. *Biomacromolecules* **2011**, *12* (3), 650–659.
(29) Azzam, F.; Galliot, M.; Putaux, J.-L.; Heux, L.; Jean, B. *Cellulose* **2015**, *22* (6), 3701–3714.
(30) Tatsumi, D.; Ishioka, S.; Matsumoto, T. *Nihon Reoroji Gakkaishi* **1999**, *27* (4), 243–248.
(31) Naderi, A.; Lindström, T.; Pettersson, T. *Cellulose* **2014**, *21* (4), 2357–2368.
(32) Derakhshandeh, B.; Kerekes, R. J.; Hatzikiriakos, S. G.; Bennington, C. P. J. *Chem. Eng. Sci.* **2011**, *66* (15), 3460–3470.
(33) Martoïa, F.; Perge, C.; Dumont, P. J. J.; Orgéas, L.; Fardin, M. A.; Manneville, S.; Belgacem, M. N. *Soft Matter* **2015**, *11* (24), 4742–4755.
(34) Dimic-Misic, K.; Nieminen, K.; Gane, P. A. C.; Maloney, T.; Sixta, H.; Paltakari, J. *Appl. Rheol.* **2014**, *24* (3), 35616.

(35) Lavoine, N.; Desloges, I.; Dufresne, A.; Bras, J. *Carbohydr. Polym.* **2012**, *90* (2), 735–764.
(36) Naderi, A.; Lindström, T. In *Cellulose and Cellulose Derivatives: Synthesis, Modification and Applications*; Mondal, M. I. H., Ed.; Nova Science Publishers, Inc., 2015; pp 187–204.
(37) Taheri, H.; Samyn, P. In *Agricultural Biomass Based Potential Materials*; Hakeem, K. R., Jawaid, M., Alothman, O. Y., Eds.; Springer International Publishing, 2015; pp 259–291.
(38) Nechyporchuk, O.; Belgacem, M. N.; Pignon, F. *Cellulose* **2015**, *22* (4), 2197–2210.
(39) Lowys, M.-P.; Desbrières, J.; Rinaudo, M. *Food Hydrocoll.* **2001**, *15* (1), 25–32.
(40) Lasseuguette, E.; Roux, D.; Nishiyama, Y. *Cellulose* **2008**, *15* (3), 425–433.
(41) Agoda-Tandjawa, G.; Durand, S.; Berot, S.; Blassel, C.; Gaillard, C.; Garnier, C.; Doublier, J.-L. *Carbohydr. Polym.* **2010**, *80* (3), 677–686.
(42) Charani, P. R.; Dehghani-Firouzabadi, M.; Afra, E.; Shakeri, A. *Cellulose* **2013**, *20* (2), 727–740.
(43) Nechyporchuk, O.; Belgacem, M. N.; Pignon, F. *Carbohydr. Polym.* **2014**, *112*, 432–439.
(44) Dimic-Misic, K.; Puisto, A.; Gane, P.; Nieminen, K.; Alava, M.; Paltakari, J.; Maloney, T. *Cellulose* **2013**, *20* (6), 2847–2861.
(45) Tatsumi, D.; Ishioka, S.; Matsumoto, T. *J. Soc. Rheol. Jpn.* **2002**, *30* (1), 27–32.
(46) Naderi, A.; Lindström, T.; Sundström, J. *Cellulose* **2014**, *21* (3), 1561–1571.
(47) Saito, T.; Uematsu, T.; Kimura, S.; Enomae, T.; Isogai, A. *Soft Matter* **2011**, *7* (19), 8804–8809.
(48) Quennouz, N.; Hashmi, S. M.; Choi, H. S.; Kim, J. W.; Osuji, C. O. *Soft Matter* **2015**, *12* (1), 157–164.
(49) Jowkarderis, L.; van de Ven, T. G. M. *Carbohydr. Polym.* **2015**, *123*, 416–423.
(50) Kroy, K.; Frey, E. *Phys. Rev. Lett.* **1996**, *77* (2), 306–309.
(51) MacKintosh, F. C.; Käs, J.; Janmey, P. A. *Phys. Rev. Lett.* **1995**, *75* (24), 4425–4428.
(52) Hill, R. J. *Biomacromolecules* **2008**, *9* (10), 2963–2966.
(53) Li, M.-C.; Wu, Q.; Song, K.; Lee, S.; Qing, Y.; Wu, Y. *ACS Sustain. Chem. Eng.* **2015**, *3* (5), 821–832.
(54) Saarinen, T.; Lille, M.; Seppälä, J. *Annu. Trans. Nord. Rheol. Soc.* **2009**, *17*.
(55) Shogren, R. L.; Peterson, S. C.; Evans, K. O.; Kenar, J. A. *Carbohydr. Polym.* **2011**, *86* (3), 1351–1357.
(56) Benhamou, K.; Dufresne, A.; Magnin, A.; Mortha, G.; Kaddami, H. *Carbohydr. Polym.* **2014**, *99*, 74–83.
(57) Taheri, H.; Samyn, P. *Cellulose* **2016**, 1–18.
(58) Saarikoski, E.; Saarinen, T.; Salmela, J.; Seppälä, J. *Cellulose* **2012**, *19* (3), 647–659.
(59) Tanaka, R.; Saito, T.; Hänninen, T.; Ono, Y.; Hakalahti, M.; Tammelin, T.; Isogai, A. *Biomacromolecules* **2016**.
(60) Bäckström, M.; Bolivar, S.; Paltakari, J. *O Pap. Rev. Mens. Tecnol. Em Celul. E Pap.* **2012**, *73* (7), 57–65.
(61) Herrick, F. W.; Casebier, R. L.; Hamilton, J. K.; Sandberg, K. R. *J. Appl. Polym. Sci. Appl. Polym. Symp.* **1983**, *37*, 797–813.
(62) Grüneberger, F.; Künniger, T.; Zimmermann, T.; Arnold, M. *Cellulose* **2014**, *21* (3), 1313–1326.
(63) Besbes, I.; Alila, S.; Boufi, S. *Carbohydr. Polym.* **2011**, *84* (3), 975–983.
(64) Naderi, A.; Lindström, T. *Cellulose* **2014**, *21* (5), 3507–3514.

(65) Iotti, M.; Gregersen, Ø. W.; Moe, S.; Lenes, M. *J. Polym. Environ.* **2011**, *19* (1), 137–145.
(66) Yang, X. H.; Zhu, W. L. *Cellulose* **2007**, *14* (5), 409–417.
(67) Ishii, D.; Saito, T.; Isogai, A. *Biomacromolecules* **2011**, *12* (3), 548–550.
(68) Ishii, D.; Saito, T.; Isogai, A. *Biomacromolecules* **2012**, *13* (5), 1706–1706.
(69) Iwamoto, S.; Lee, S.-H.; Endo, T. *Polym. J.* **2014**, *46* (1), 73–76.
(70) Tanaka, R.; Saito, T.; Ishii, D.; Isogai, A. *Cellulose* **2014**, *21* (3), 1581–1589.
(71) Tanaka, R.; Saito, T.; Hondo, H.; Isogai, A. *Biomacromolecules* **2015**, *16* (7), 2127–2131.
(72) Dinand, E.; Chanzy, H.; Vignon, M. R. *Cellulose* **1996**, *3* (1), 183–188.
(73) Mohtaschemi, M.; Dimic-Misic, K.; Puisto, A.; Korhonen, M.; Maloney, T.; Paltakari, J.; Alava, M. J. *Cellulose* **2014**, *21* (3), 1305–1312.
(74) Karppinen, A.; Vesterinen, A.-H.; Saarinen, T.; Pietikäinen, P.; Seppälä, J. *Cellulose* **2011**, *18* (6), 1381–1390.
(75) Karppinen, A.; Saarinen, T.; Salmela, J.; Laukkanen, A.; Nuopponen, M.; Seppälä, J. *Cellulose* **2012**, *19* (6), 1807–1819.
(76) Bettaieb, F.; Nechyporchuk, O.; Khiari, R.; Mhenni, M. F.; Dufresne, A.; Belgacem, M. N. *Carbohydr. Polym.* **2015**, *134*, 664–672.
(77) Saarinen, T.; Haavisto, S.; Sorvari, A.; Salmela, J.; Seppälä, J. *Cellulose* **2014**, *21* (3), 1261–1275.
(78) Barnes, H. A. *J. Non-Newton. Fluid Mech.* **1995**, *56* (3), 221–251.
(79) Ovarlez, G.; Rodts, S.; Chateau, X.; Coussot, P. *Rheol. Acta* **2009**, *48* (8), 831–844.
(80) Manneville, S.; Bécu, L.; Colin, A. *Eur. Phys. J. - Appl. Phys.* **2004**, *28* (3), 361–373.
(81) Haavisto, S.; Koponen, A. I.; Salmela, J. *Chem. Eng.* **2014**, *2*, 27.
(82) de Kort, D.; Veen, S. J.; As, H. van; Bonn, D.; Velikov, K. P.; Duynhoven, J. van. *Soft Matter* **2016**, *12*, 4739–4744.

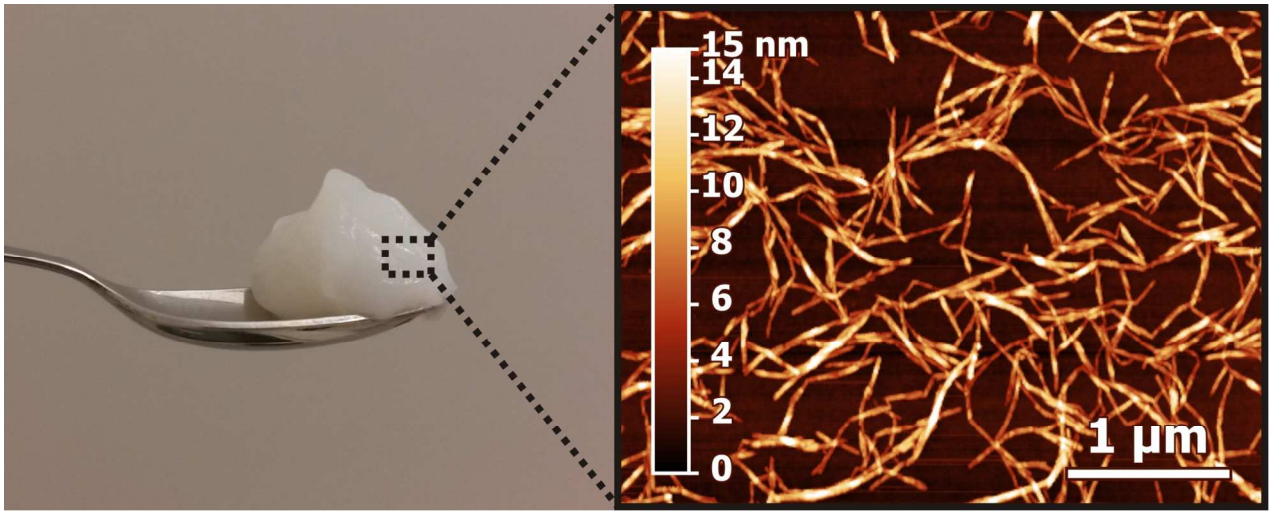

Table of Contents Graphic

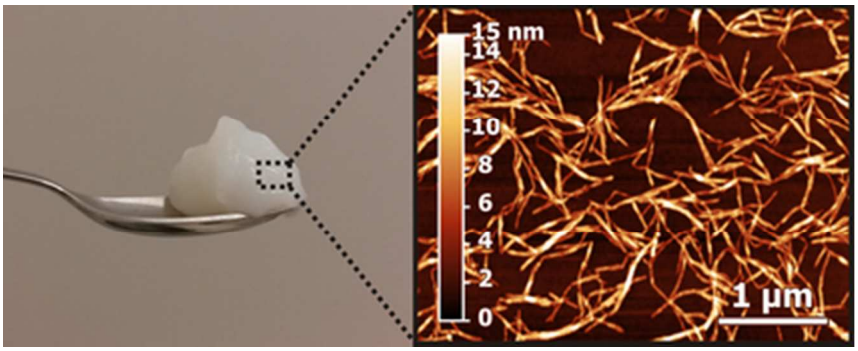

Table of Contents graphic
35x14mm (300 x 300 DPI)

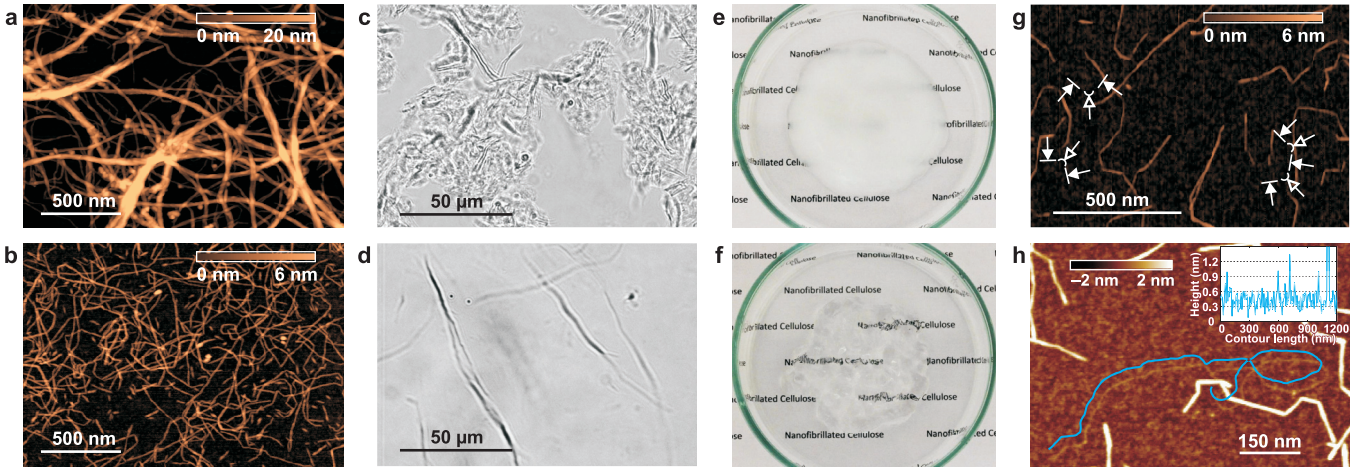
a
0 nm 20 nm
500 nm
c
50 µm
e
Nanofibrillated Cellulose
g
0 nm 6 nm
500 nm
b
0 nm 6 nm
500 nm
d
50 µm
f
Nanofibrillated Cellulose
h
–2 nm 2 nm
Height (nm)
1.2
0.9
0.6
0.3
0
0 300 600 900 1200
Contour length (nm)
150 nm

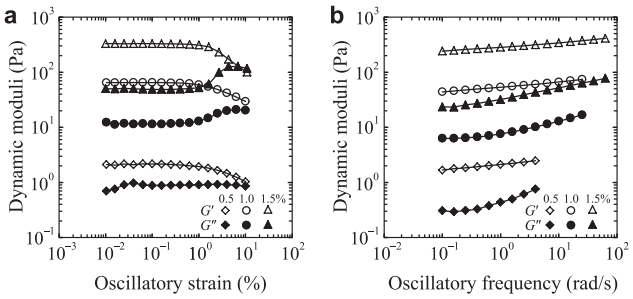
a
b
Dynamic moduli (Pa)
Oscillatory strain (%)
Oscillatory frequency (rad/s)
G′
G″
0.5 1.0 1.5%

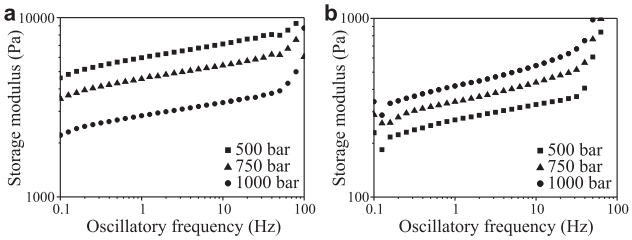
a
10000
1000
Storage modulus (Pa)
0.1
1
10
100
Oscillatory frequency (Hz)
500 bar
750 bar
1000 bar
b
1000
100
Storage modulus (Pa)
0.1
1
10
100
Oscillatory frequency (Hz)
500 bar
750 bar
1000 bar

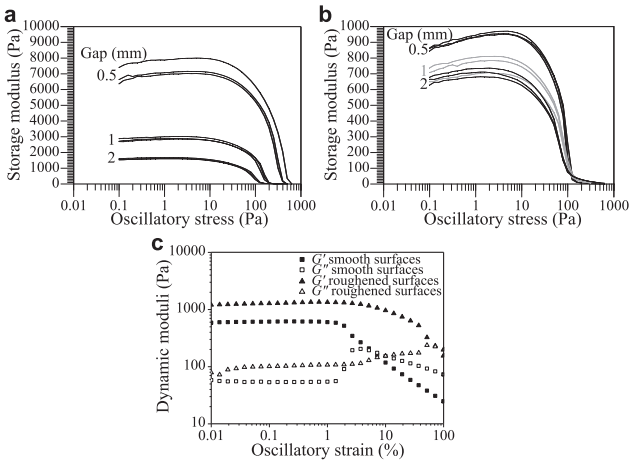
a
Storage modulus (Pa)
Gap (mm)
0.5
1
2
Oscillatory stress (Pa)
b
Storage modulus (Pa)
Gap (mm)
0.5
1
2
Oscillatory stress (Pa)
c
Dynamic moduli (Pa)
G′ smooth surfaces
G″ smooth surfaces
G′ roughened surfaces
G″ roughened surfaces
Oscillatory strain (%)

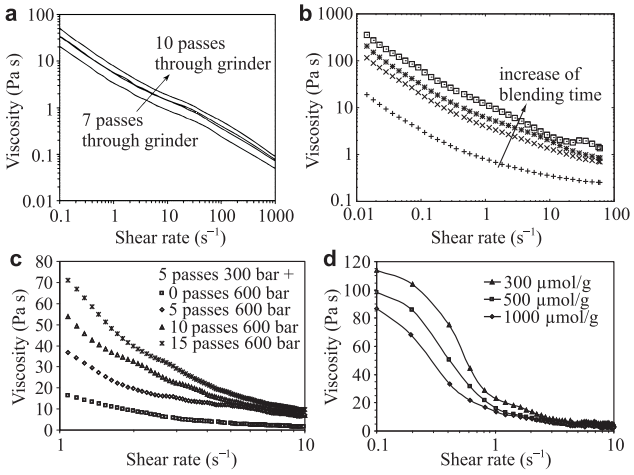
a
Viscosity (Pa s)
Shear rate (s⁻¹)
10 passes through grinder
7 passes through grinder
b
Viscosity (Pa s)
Shear rate (s⁻¹)
increase of blending time
c
Viscosity (Pa s)
Shear rate (s⁻¹)
5 passes 300 bar +
0 passes 600 bar
5 passes 600 bar
10 passes 600 bar
15 passes 600 bar
d
Viscosity (Pa s)
Shear rate (s⁻¹)
300 µmol/g
500 µmol/g
1000 µmol/g

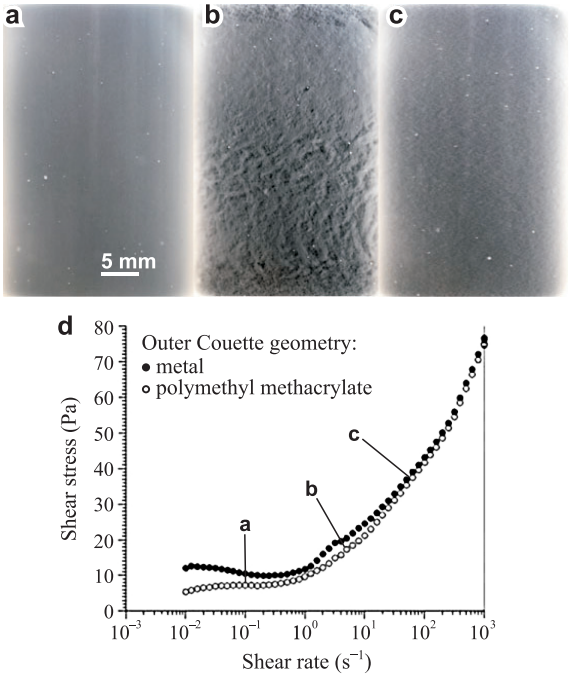
a
b
c
5 mm
d
Outer Couette geometry:
metal
polymethyl methacrylate
Shear stress (Pa)
Shear rate (s^{-1})
a
b
c

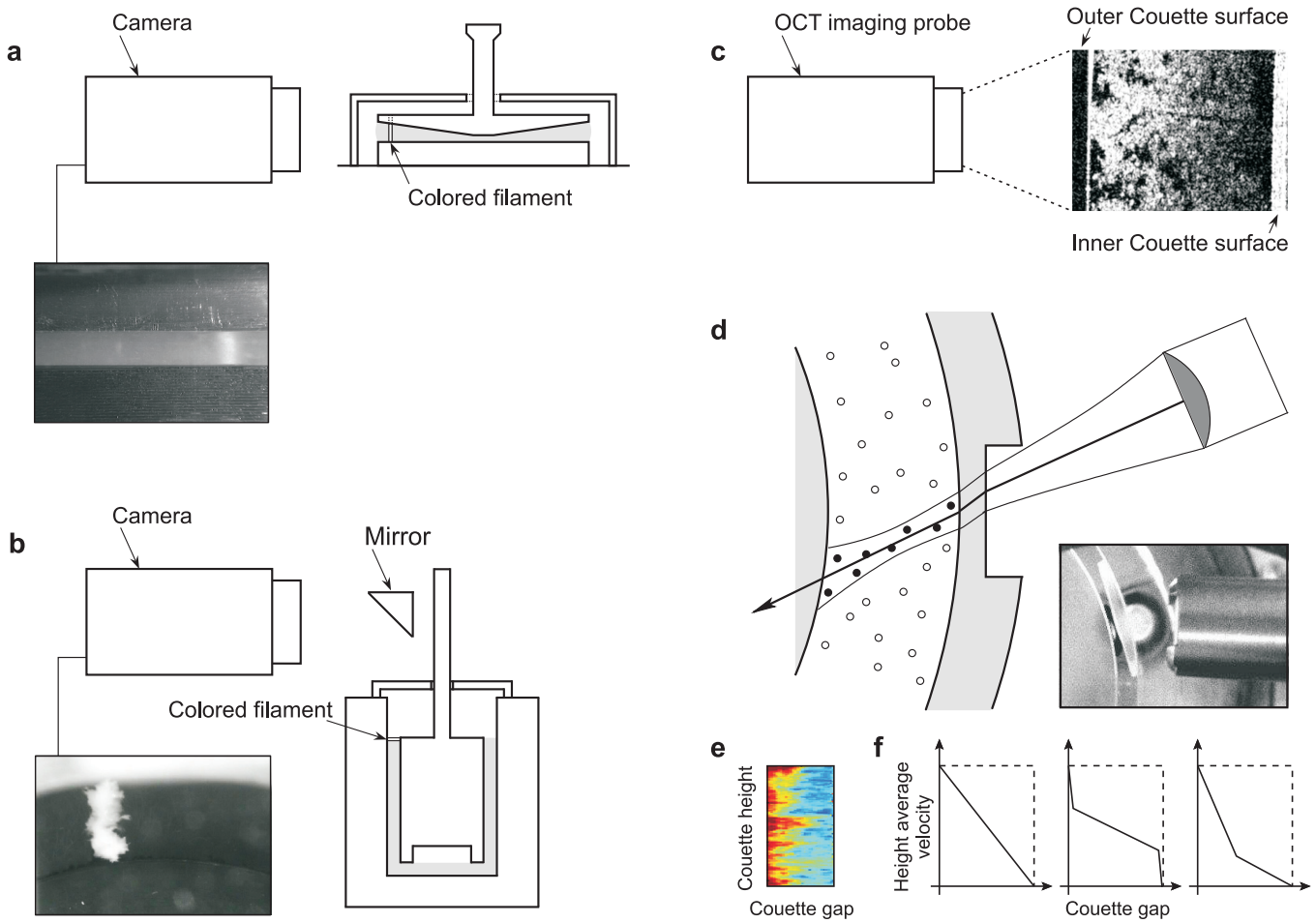
a
Camera
Colored filament
b
Camera
Mirror
Colored filament
c
OCT imaging probe
Outer Couette surface
Inner Couette surface
d
e
Couette height
Couette gap
f
Height average velocity
Couette gap

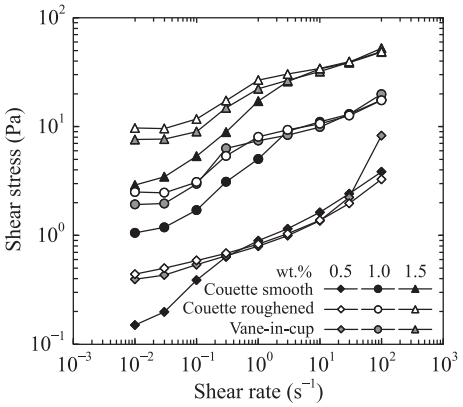
Shear stress (Pa)
Shear rate (s^{-1})
wt.% 0.5 1.0 1.5
Couette smooth
Couette roughened
Vane-in-cup

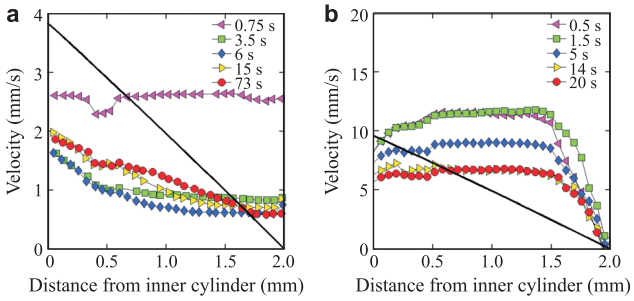
a
b
0.75 s
3.5 s
6 s
15 s
73 s
0.5 s
1.5 s
5 s
14 s
20 s
Velocity (mm/s)
Distance from inner cylinder (mm)